Mon. Not. R. Astron. Soc. **000**, 1–7 (2014) Printed 24 April 2015 (MN LATEX style file v2.2)

Correlation between star formation activity and electron density of ionized gas at z=2.5

Rhythm Shimakawa[1,2⋆], Tadayuki Kodama[2,3], Charles C. Steidel[4], Ken-ichi Tadaki[5], Ichi Tanaka[1], Allison L. Strom[4], Masao Hayashi[3], Yusei Koyama[6], Tomoko L. Suzuki[2], and Moegi Yamamoto[2]

[1] *Subaru Telescope, National Astronomical Observatory of Japan, N. A′ohoku Pl., Hilo, HI 96720, USA*
[2] *Department of Astronomical Science, SOKENDAI (The Graduate University for Advanced Studies), Osawa, Mitaka, Tokyo 181-8588, Japan*
[3] *Optical and Infrared Astronomy Division, National Astronomical Observatory, Mitaka, Tokyo 181-8588, Japan*
[4] *Department of Astronomy, California Institute of Technology, E. California Blvd., Pasadena, CA 91125, USA*
[5] *Max-Planck-Institut für Extraterrestrische Physik, Giessenbachstrasse, D-85748 Garching, Germany*
[6] *Institute of Space Astronomical Science, Japan Aerospace Exploration Agency, Sagamihara, Kanagawa, 252-5210, Japan*

Accepted 2015 April 22. Received 2015 March 25; in original form 2014 November 5

ABSTRACT

In the redshift interval of $2 < z < 3$, the physical conditions of the inter-stellar medium (ISM) in star-forming galaxies are likely to be different from those in the local Universe because of lower gaseous metallicities, higher gas fractions, and higher star formation activities. In fact, observations suggest that higher electron densities, higher ionization parameters, and harder UV radiation fields are common.

In this paper, based on the spectra of Hα-selected star-forming galaxies at $z = 2.5$ taken with Multi-Object Spectrometer for InfraRed Exploration (MOSFIRE) on Keck-1 telescope, we measure electron densities (n_e) using the oxygen line ratio ([OII]$\lambda\lambda$3726,3729), and investigate the relationships between the electron density of ionized gas and other physical properties. As a result, we find that the specific star formation rate (sSFR) and the surface density of SFR ($\Sigma_{\rm SFR}$) are correlated with the electron density at $z = 2.5$ for the first time. The $\Sigma_{\rm SFR}$–n_e relation is likely to be linked to the star formation law in HII regions (where star formation activity is regulated by interstellar pressure). Moreover, we discuss the mode of star formation in those galaxies. The correlation between sSFR and $\Sigma_{\rm SFR}$ suggests that highly star-forming galaxies (with high sSFR) tend to be characterized by higher surface densities of star formation ($\Sigma_{\rm SFR}$) and thus higher n_e values as well.

Key words: galaxies: formation — galaxies: high-redshift — galaxies: ISM

1 INTRODUCTION

After the recent advent of high sensitivity, multi-object near-infrared (NIR) spectrographs typified by MOSFIRE on the Keck telescope and KMOS (The K-band Multi Object Spectrograph) on the Very Large Telescope, physical properties of high-z star-forming (SF) galaxies explored by deep spectroscopy have been hot issues with the initial burst of available data that are being accumulated (Holden et al. 2014; Steidel et al. 2014; Shapley et al. 2015; Coil et al. 2015). Most work has focused on the mass–metallicity relations (Tremonti et al. 2004; Sanders et al. 2015), the improved BPT diagrams (Baldwin et al. 1981; Steidel et al. 2014; Shapley et al. 2015) and MEx diagrams (Juneau et al. 2011, 2014) of SF galaxies at high redshifts. These analyses are now producing good measurements of gaseous excitation levels and metallicities of those galaxies. In particular, recent large on-going programs such as KBSS-MOSFIRE (Strom et al. in prep.) and MOSDEF (Kriek et al. 2014) will soon provide us with NIR spectra of ∼1000 galaxies, all with reasonably high-quality spectra.

However, so far most published analyses have not investigated another important parameter, that is the electron density n_e at $z > 2$. The electron density can be estimated from the ratios of collisonally-excited metal lines [OII]$\lambda\lambda 3726, 3729$ or [SII]$\lambda\lambda 6717, 6731$ doublets (Osterbrock

⋆ E-mail: rhythm@naoj.org

1974). This is a reliable physical quantity that is free of issues with flux calibration, is largely independent of metallicity, and only weakly depends on electron temperature. One matter for concern is that [SII] line should come from outer part of HII region or photo-dissociation region (PDR, Hollenbach & Tielens 1999) compared to [OII] line. Thus the [OII] doublet is in favor of measuring n_e accurately.

Some recent measurements suggest that the electron densities of high-z (z>2) galaxies tend to have $n_e \sim 30 - 1000$ /cm^3 (Lehnert et al. 2009; Masters et al. 2014; Steidel et al. 2014), a range in which n_e is sensitive to [OII] and [SII] line ratios which then enables us to investigate electron densities in high-z galaxies. Shirazi et al. (2014) have reported that high-z galaxies tend to have higher n_e than those of low-z counterparts for given sSFR and stellar mass, based on the indirect measurement (see the details in the literature).

This paper presents n_e measurements, based on the [OII] doublet by deep NIR spectroscopy of SF galaxies at $z = 2.5$ obtained with MOSFIRE. The electron density provides information on ISM conditions on scales much smaller than most of the measurements of gas surface density used in the context of the Kennicutt-Schmidt (KS) relation (Schmidt 1959; Kennicutt 1998; Kennicutt & Evans 2012). In the past decade, Liu et al. (2008) have suggested that ISM condition is controlled by star formation intensities, and Brinchmann et al. (2008) have shown the correlation between specific star formation rate (sSFR) and electron density from the [SII] doublet lines at $z \sim 0.1$ for the first time. However no statistical study of electron density of SF galaxies at $z > 2$ has been conducted so far. We present here the first of such analysis and show some intriguing correlations found between star formation and electron density of ionized gas at $z > 2$ with the reliable, direct [OII] measurements. We assume the cosmological parameters of Ω_M=0.3, Ω_Λ=0.7 and H_0=70 km/s/Mpc and employ a Chabrier (2003) stellar initial mass function (IMF).

2 OBSERVATION, ANALYSES, AND DATA

2.1 Observation and analyses

We selected our MOSFIRE spectroscopic targets from 68 Hα emitters (HAEs) associated with a protocluster, USS 1558–003 at $z = 2.53$ (Hayashi et al. 2012) (hereafter USS1558). These are constructed from our previous narrow-band (NB) imaging survey with NB2315 ($\lambda_{\rm center}$=2317 nm and FWHM=26 nm) with MOIRCS (Multi-Object Infrared Camera and Spectrograph; Ichikawa et al. 2006; Suzuki et al. 2008) on the Subaru telescope on Mauna Kea, as a part of the MAHALO-Subaru project (Mapping HAlpha and Lines of Oxygen with Subaru; Kodama et al. 2013). The HAEs are first selected as those showing excess in NB flux above the 3σ level, and equivalent widths greater than 20Å in the rest frame. We then apply a broad-band colour-colour diagram ($r'JK_s$) in order to reduce fore- or background contamination from [OIII]/[OII]/Paα emitters at some other redshifts (see more detail in Hayashi et al. 2012). Moreover, we placed higher priorities on the 36 objects which had been confirmed spectroscopically by our previous NIR spectroscopic observations with MOIRCS (Shimakawa et al. 2014, 2015).

Spectroscopic observations were carried out in June 2014 with MOSFIRE, a near-infrared imager and spectrograph (McLean et al. 2010, 2012) on the Keck-1 telescope on Mauna Kea. A mask was created with 26 slits (each 0"7 wide) including 20 main targets, 5 galaxies consisting of 2 NB emitters deselected by colour-colour diagram in Hayashi et al. (2012) or 3 objects at photometric redshifts of z=1–2 by EASY (Brammer et al. 2008), and a star to monitor atmosphere conditions. The observation was set with the ABA'B' dither pattern of individual exposure time of 120s in both J- and H-bands. We integrated for 3hrs in J- and H-bands each under 0.5–0.7 arc sec seeing size (FWHM). The J- and H-band modes of MOSFIRE provide high spectral resolutions of R=3318 and 3660 in the range of λ=1.17–1.35 and 1.47–1.80 μm, respectively, enabling us to resolve the [OII] doublet in J-band at z=2.5.

The spectra were reduced using the MOSFIRE Data Reduction Pipeline (MOSFIRE-DRP), described in more detail by Steidel et al. (2014). This software uses standard data reduction procedures and produces a scientific 2D spectrum for each target. The flux calibration was conducted by using a standard star, HD 199217 with an A0V spectrum.

17 out of 20 of our target HAEs show more than one emission line, such as [OIII], Hβ, Hγ and [OII] at the protocluster redshift that are detected above the 5 sigma flux limit. We have conducted a Gaussian fitting for the [OII] and [OIII] lines wherever available, using the spectral fitting software SPECFIT (Kriss 1994) distributed within STSDAS[1] in the IRAF[2] environment. We assumed two Gaussian components with the same line width to fit the respective [OII] and [OIII] lines at the fixed wavelengths of 3727.1/3729.9 Å for the [OII] doublet and 4960.3/5008.2 Å for the [OIII] doublet. We also fixed [OIII] line ratio at [OIII]λ5007/[OIII]λ4959=3 (Storey & Zeippen 2000). The wavelength dependent sky Poisson noise that is largely affected by the presence of OH sky lines is also taken into account in the line fitting, and thus the fitting results should properly incorporate the observational uncertainties and the fitting errors. Obtained flux of these emission lines show the values between 0.5×10^{-17} and 10×10^{-17} erg/s/cm^2 and those S/N ratios are above 3.2σ. Typical line fluxes (and S/N levels) are [OIII]λ5007=3.6 $\times$ 10^{-17} erg/s/cm^2 (15σ), Hβ=1.0 $\times$ 10^{-17} erg/s/cm^2 (9σ) and [OII]$\lambda\lambda$3726+3729=2.6 $\times$ 10^{-17} erg/s/cm^2 (11σ), respectively. Median 1σ line flux uncertainties are 1.6×10^{-18} and 1.8×10^{-18} erg/s/cm^2 in J and H bands. For 3 of 17 targets, one of the two [OII] lines is severely affected by OH sky lines unfortunately, and thus the ratio could not be measured. Hereafter we do not include these galaxies in the analyses. Our final sample therefore consists of 14 HAEs at $z = 2.5$. All line spectra are presented in Fig. 1.

The electron density is then calculated for each HAE based on the measured intensity ratio of the [OII] doublet using the TEMDEN code distributed in the STSDAS package. The determination of the electron density depends weakly on the electron temperature, and we assume the fixed value of 10 000 K (Osterbrock 1974) because independent mea-

[1] Available at www.stsci.edu/institute/software_hardware/stsdas/
[2] IRAF is distributed by National Optical Astronomy Observatory and available at iraf.noao.edu/

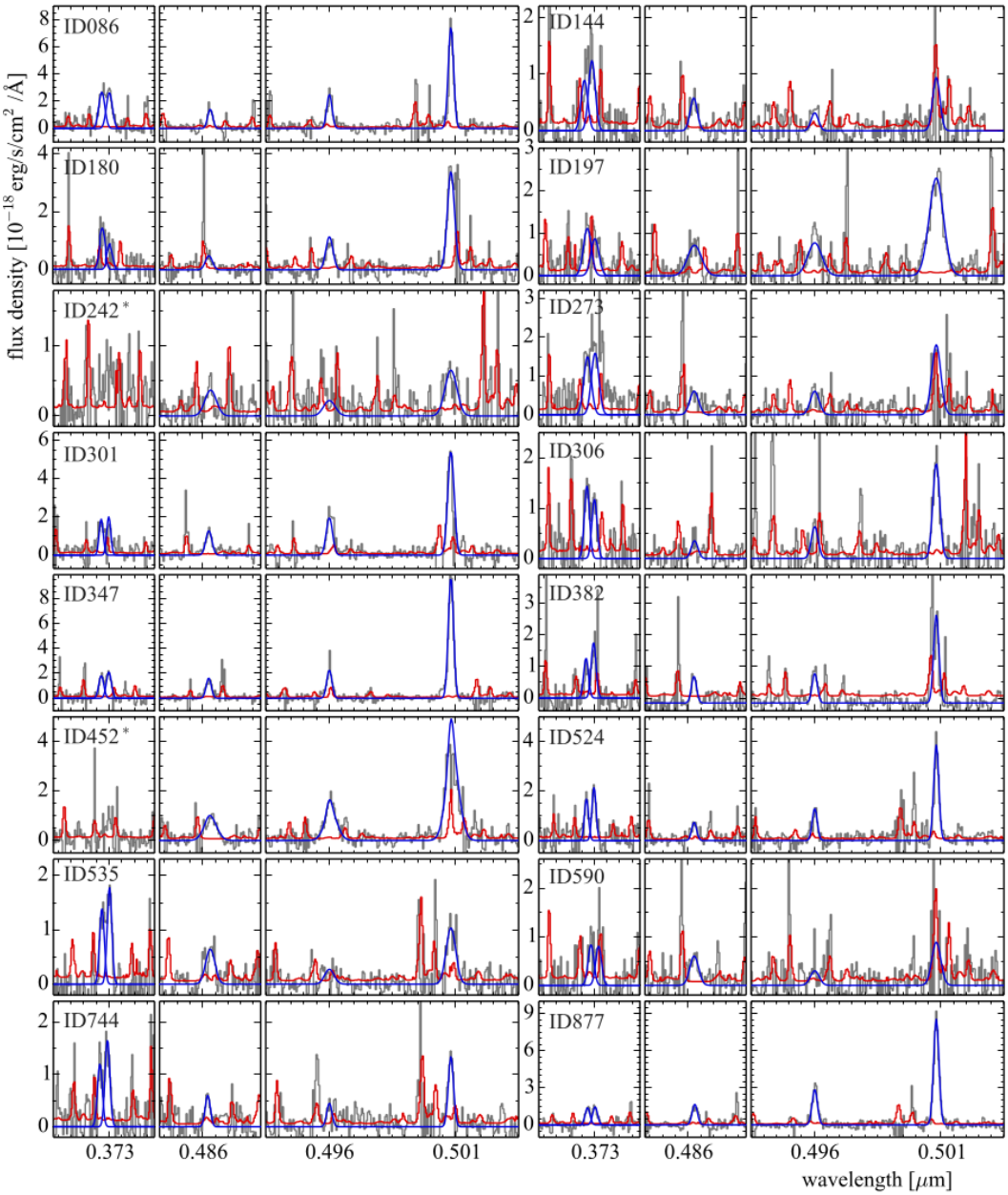

Figure 1. Spectra of our HAEs at z=2.5. In each panel, black, red and blue lines show the reduced spectrum, sky Poisson noise and the best fit curve to the [OII]$\lambda\lambda$3726, 3729, H$\beta\lambda$4861, and [OIII]$\lambda\lambda$4959, 5007 lines, respectively. Two HAEs (ID242, 452) for which [OII] doublet lines cannot be fit are excluded from our sample.

surements are not available. Note however that the choice of this value does not affect our conclusions.

2.2 Slit loss correction, stellar mass, and SFR

In order to obtain absolute line flux $F_{int,obj}$, we correct for the slit loss by the following equation,

$$F_{int,obj} = \frac{F_{int,star}}{F_{obs,star}} \times \frac{f_{loss,star}}{f_{loss,obj}} \times F_{obs,obj}, \qquad (1)$$

where $F_{int,star}$ and $F_{obs,star}$ are the intrinsic flux derived from J- or H-band image and the observed flux of the monitoring star placed on our slit mask used for spectroscopy. $f_{loss,star}$ is a slit loss of the monitoring star. Here we assume its value of 0.76 and 0.80 in J- and H-bands which correspond to 0"70 and 0"65 of seeing size in FWHM, respectively. $f_{loss,obj}$ is the slit loss of our science targets and is estimated by assuming the single Gaussian component that is spilt outside of the 0"7 slit width for each FWHM based on the NB image (Hayashi et al. 2012). $f_{loss,obj}$ is distributed between 0.42 and 0.78, and a median value is 0.69. This correction may cause a large uncertainty for those having multiple HII regions as pointed out by Kriek et al. (2014). Therefore we double-check this effect by comparing the [NII]-corrected NB fluxes with the spectroscopic Hα line fluxes of 28 HAEs at z = 2.5 (of which 10 are common in this work) measured from our previous MOIRCS spectra (Shimakawa et al. 2015). The [NII] correction is calibrated as a function of stellar mass as is applied in Shimakawa et al. (2015). The result shows the typical uncertainty including

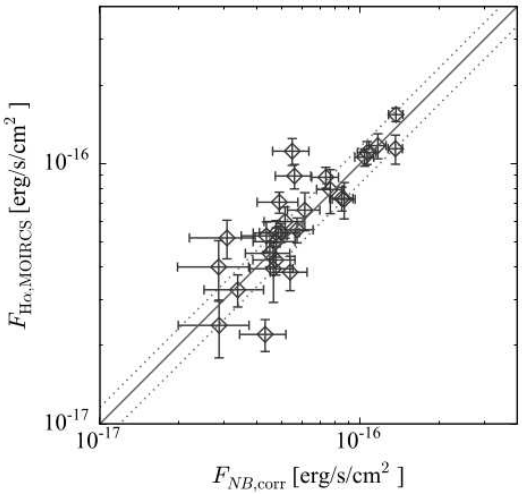

Figure 2. Comparison between slit-loss corrected Hα line fluxes and [NII]-corrected NB fluxes for HAEs at z=2.5 in Shimakawa et al. (2015). Solid and dotted lines show a 1:1 line and the median scatter of 16%, respectively.

the [NII] correction is 16% (Fig. 2). We ignore this small error hereafter, since this paper only discuss the statistical properties of the sample.

We use the photometric data ($Br'z'JHK_s$ and NB) catalog of Hayashi et al. (2012) in order to obtain stellar masses and SFRs of the individual galaxies. The stellar masses are derived from the FAST, SED-fitting program (Kriek et al. 2009) using the stellar population model of Bruzual & Charlot (2003), the Calzetti et al. (2000) extinction curve, and the Chabrier (2003) IMF. We fix the metallicity to the solar value for the SED models and assume an delayed exponentially declining star formation history ($\sim t\exp(-t/\mathrm{tau})$) with the fixed time-scale of $\log(\tau/\mathrm{yr})$=8.4. The SFRs are calculated from Hα luminosity by using the Kennicutt (1998) prescription but with Chabrier (2003) IMF. We have corrected for the nebular dust extinction based on the Balmer decrement (Hα/ Hβ=2.86) by assuming a Case-B recombination in the gas temperature of T_e=10^4 K and the electron density of n_e=10^2 cm^{-3} (Brocklehurst 1971), as well as assuming the Calzetti et al. (2000) extinction curve for [OII] and [OIII] lines. Hα and Hβ fluxes are derived from the [NII]-corrected NB flux and the spectroscopic Hβ line flux whose slit loss is rectified as mentioned above.

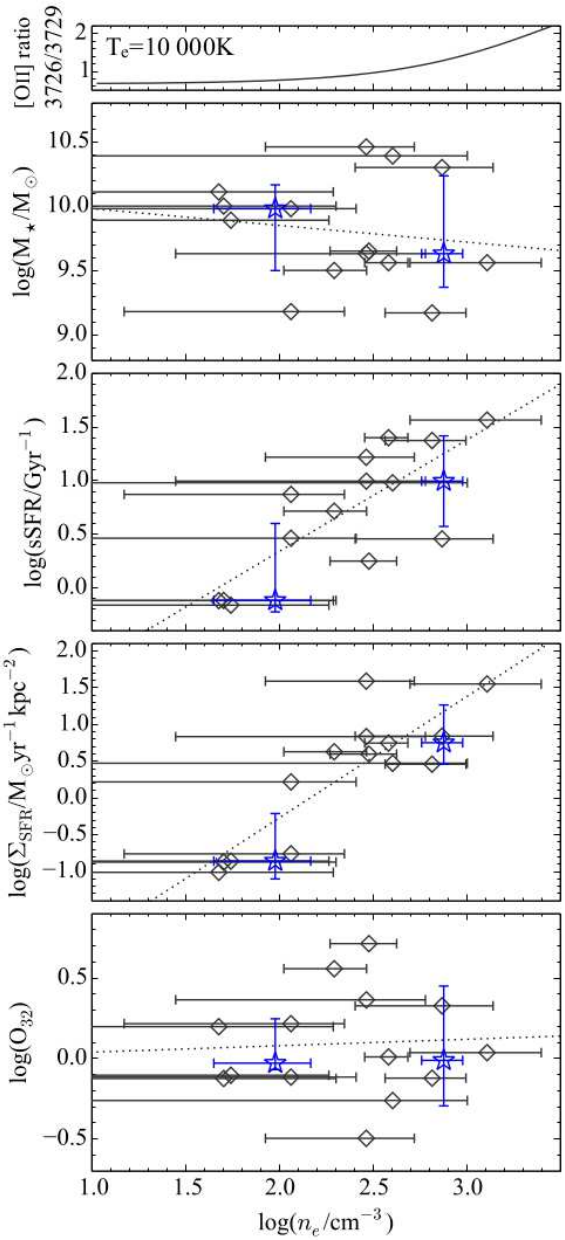

Figure 3. From top, log (a) [OII]$\lambda\lambda$3726, 3729 line ratio, (b) stellar mass, (c) sSFR, (d) $\Sigma_{\rm SFR}$ and (e) O_{32} as a function of log electron density. Diamonds indicate our sample, HAEs at z = 2.5. Errorbars of n_e are determined from flux errors of [OII]$\lambda\lambda$3726, 3729. Blue star symbols represent n_e of the stacked data separated by n_e = 160 cm^{-3} and those y-values show median values and 1σ scatters. Dotted lines show the best fit lines for our targets.

3 RESULTS

Grounded on the datasets, this *Paper* explores the relationships of electron density (n_e) in the ionized regions with stellar mass, sSFR, SFR surface density ($\Sigma_{\rm SFR}$) and [OIII]/ [OII] line ratio. $\Sigma_{\rm SFR}$ is defined by SFR/$\pi r_{\rm eff}^2$ where $r_{\rm eff}$ is the effective radius of a NB image profile for each object. We derive $r_{\rm eff}$ from the NB image (seeing 0"4 FWHM) by using the GALFIT VERSION 3.0 code (Peng et al. 2010). Here, we employed only the NB data with good seeing sizes among the data used in Hayashi et al. (2012). The seeing-limited data may cause a large uncertainty of $r_{\rm eff}$ for the galaxies which remain unresolved in some cases. However, our conclusion remains the same even if we exclude those small, unresolved galaxies. The median effective radius is $r_{\rm eff}$=2.1 kpc which corresponds to 0.26 arc sec.

Figure 3 represents (a) [OII]$\lambda\lambda$3726, 3729 line ratio, log (b) stellar mass, (c) sSFR, (d) surface density of SFR and (e) [OIII]/ [OII] line ratio ($O_{32}\equiv$ [OIII]$\lambda\lambda$4959, 5007/ [OII]$\lambda\lambda$3726, 3729) as a function of log electron density. All physical parameters are dust-corrected by using the Balmer decrement and the Calzetti et al. (2000) extinction curve (§2.2). First of all, as seen in the Fig. 3a, the [OII]$\lambda\lambda$3726, 3729 line ratio is

Table 1. Fitted slopes (N) and those standard errors to the HAEs on log stellar mass, sSFR, $\Sigma_{\rm SFR}$ or O_{32} (y) plotted against log electron density ($x \equiv \log(n_e/{\rm cm}^3)$). 3rd and 4th columns indicate Spearman's rank correlation coefficients and their significance in the respective diagram suggested for the HAEs at $z = 2.5$.

y	N	r_s	σ
$\log({\rm M}_\star/{\rm M}_\odot)$	–0.13±0.26	–0.16	1.3
$\log({\rm sSFR/Gyr}^{-1})$	1.04±0.23	0.68	4.0
$\log(\Sigma_{\rm SFR}/{\rm M}_\odot{\rm yr}^{-1}{\rm kpc}^{-2})$	1.65±0.29	0.73	4.2
$\log({\rm O}_{32})$	0.04±0.21	0.07	0.6

most sensitive for n_e>100 cm^{-3}. On the other hand, there is a large uncertainty in estimating electron density for the galaxies with low n_e since [OII] line ratio is saturated below ∼10 cm^{-3}. Measured [OII]λ3726/ [OII]λ3729 ratios show values between 0.71–1.6, and the median electron density is 291 cm^{-3}. To investigate the correlations among the physical quantities, we calculate Spearman's rank-correlation coefficients r_s and those significance. These are summarized in Table 1. Also, we check them excluding low mass galaxies ($\log({\rm M}_\star/{\rm M}_\odot)$<10) as well, in order to minimize the stellar mass dependence.

In our sample, sSFR (Fig. 3c) and SFR surface density (Fig. 3d) are both correlated with electron density with $\sim 4\sigma$ significance (Table 1). Current data show ${\rm sSFR}\propto n_e^{1.1\pm0.2}$ and $\Sigma_{\rm SFR}\propto n_e^{1.7\pm0.3}$. These power laws change depending on absorption corrections although the tight relationships remain constant. We also can see the positive correlations in two composite spectra which are separated by n_e=160 cm^{-3}. These are stacked with weight of noise ($\equiv \Sigma_i^n(fluxdensity/noise^2)/\Sigma_i^n(1/noise)^2$). On the other hand, any dependencies of stellar mass and O_{32} on electron density (Fig. 3b,e) cannot be identified due to a lack of statistics. However, we have confirmed a moderate negative correlation between log stellar mass and O_{32} with 3σ significance, which agrees with Nakajima & Ouchi (2014); Steidel et al. (2014).

4 DISCUSSION AND CONCLUSIONS

4.1 Star formation law in ionized gas

Past works have indicated the association of star formation with electron density (Martin 1997; Liu et al. 2008; Brinchmann et al. 2008; Shirazi et al. 2014). This work clearly shows quantitatively the correlation between sSFR and electron density and the one between $\Sigma_{\rm SFR}$ and electron density at $z = 2.5$ based on the reliable measurements. These relationships indicate that the interstellar pressure and the SF activities are closely linked. In particular, the n_e–$\Sigma_{\rm SFR}$ correlation should mean that the interstellar pressure controls the intensity of SF activity ($\Sigma_{\rm SFR}$) in HII regions. The electron density probes the physical 3D density of ionized SF regions, and it must be related to other 2D density measurements of molecular or neutral gases. Also a typical HII region has a lifetime of a few Myrs (comparable to the lifetime of OB stars) which is by a factor of a few – an order of magnitude shorter than that of cold gas clouds. This means that the electron density more selectively corresponds to the interstellar pressure of young star-forming regions. If the electron density is somehow related to the density of cold ISM, which is likely the case since the ionized gas originates from molecular gas, the relation between $\Sigma_{\rm SFR}$ and electron density that we see here must be closely related to the the KS law (see also Shirazi et al. 2014).

However, we need some careful considerations for the implications of this correlation. First of all, it is not necessarily the case that n_e–$\Sigma_{\rm SFR}$ correlation links to the KS law ($\Sigma_{\rm gas}$–$\Sigma_{\rm SFR}$). The measured electron density directly scales with the gas density if the hydrogen is fully-ionized and only in the SF HII regions. However, the ionized gas are not only confined in the SF regions containing young massive stars, but also seen around AGNs or in the outer diffuse gas (warm ionized medium, Oey & Kennicutt 1997; Martin 1997; Charlot & Longhetti 2001), and therefore the electron density does not necessarily correspond to the gas density of the SF regions. Secondly, [OII] line fluxes that we obtain are the surface-brightness-weighted and ensemble averaged for the entire galaxy or the part that falls into the slit of 0"7 width. In particular, the electron density is measured on quite a different scale (50–100 pc) from that of surface gas density used for the KS law (∼1 kpc). In fact, the slope of $\Sigma_{\rm SFR}$–$\Sigma_{\rm gas}$ depends on the observed scale (Oey et al. 2007; Prescott et al. 2007; Bigiel et al. 2008; Heiderman et al. 2010) and Kruijssen & Longmore (2014) have theoretically shown the scale-dependence of the KS relation. Such combined effects of the surface-brightness-weighted measurements and its scale dependence make the physical understanding of the n_e–$\Sigma_{\rm SFR}$ correlation difficult.

These problems will be solved by integral field spectroscopy assisted by adaptive optics on next generation telescopes such as Thirty Meter Telescope whose spatial resolution is as good as 100 pc at $z \sim 2$. Alternatively, local galaxies with high $\Sigma_{\rm SFR}$ will be able to provide us with crucial information even under natural seeing conditions by comparing the spatially-resolved electron density map with that of HCN, for example, which traces dense clumps with forming stars.

4.2 Relationship between sSFR and $\Sigma_{\rm SFR}$

Then, we discuss the mode of star formation in high-z galaxies based on the sSFR, $\Sigma_{\rm SFR}$, and $r_{\rm eff}$, including the data from the SINS survey (Spectroscopic Imaging survey in the near-IR with SINFONI) of high redshift galaxies (Förster Schreiber et al. 2009). This work employs their stellar masses and SFRs derived from the SED-fitting that are all available in the literature. We note that our data exactly follow the same main-sequence (i.e. relationships between stellar mass and SFR) of their sample. Therefore we analyse and plot their samples together with ours.

The results are shown in Figure 4. We can see a correlation between sSFR and SFR surface density for all the samples. The Spearman's correlation factor is calculated to r_s=0.68 which shows above 5σ significance. The sSFR indicates the strength of global SF activity like star-burstiness, while $\Sigma_{\rm SFR}$ represents more local but averaged surface density of star forming regions. Therefore this correlation suggests that the SF galaxies with higher sSFRs tend to be characterized by higher surface densities of star formation rate ($\Sigma_{\rm SFR}$) probably due to higher cold gas densities according to the KS law. It is also probably connected to higher

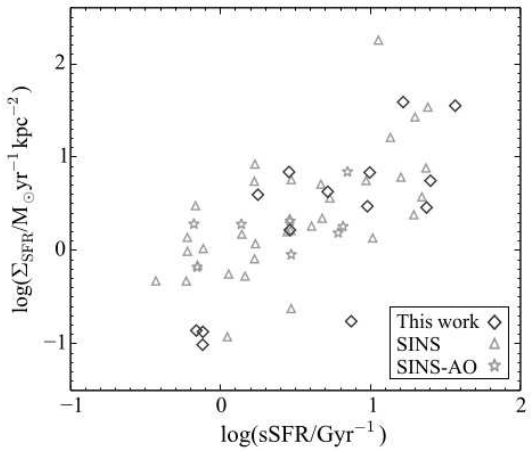

Figure 4. Log sSFR versus SFR surface density. Along with the data of this work (the same plots as in Fig. 3), triangles and star marks represent SF galaxies at $z \sim 2$ in the SINS survey (Förster Schreiber et al. 2009). The star marks indicate those whose $r_{\rm eff}$ are derived from AO-assisted IFU observations.

electron densities. This may be understood if we consider that a burst-like intense star formation tends to occur in a central compact region (see also Wuyts et al. 2011).

Finally, we should note that our sample is biased to HAEs at $z = 2.5$ in the protocluster environment. This means that environmental effects on feeding and feedback in galaxy formation may influence the chemical evolution of SF galaxies even at the fixed stellar mass (Kulas et al. 2013; Shimakawa et al. 2015; Valentino et al. 2015). It may cause a large scatter in O32, since O32 is not only dependent on ionization parameter, but also gaseous metallicity. Furthermore, it is expected that the mode of star formation depends on environment. For example, galaxy-galaxy interactions occur more frequently in cluster environment (Gottlöber et al. 2001). The model of SF in cluster galaxies could be different due to more frequent nuclear starbursts by major mergers. However, this effect is largely independent of the correlations found in this *Paper*, since our sample follow the same sequence of SF galaxies studied by SINS survey in the diagrams between sSFR and $\Sigma_{\rm SFR}$.

In summary, this paper shows and discusses the star formation law in ionized gas characterized by the n_e–$\Sigma_{\rm SFR}$ correlation for the first time. So far, the accurate slope and its physical understanding remain unclear, and more statistical and coherent sample is required. To achieve this, MOSFIRE is a powerful spectrograph which has good enough sensitivity to detect and resolve [OII] doublet lines for individual galaxies at high-z at reasonably high S/N levels. Large programs such as KBSS, MOSDEF and the other ongoing projects using MOSFIRE have already started and will be able to shed light in the physical states of star forming galaxies at the peak epoch of galaxy formaiton.

ACKNOWLEDGMENTS

We are grateful to the anonymous referee for useful comments. The data presented in this paper were obtained at the W. M. Keck Observatory, which is operated as a scientific partnership among the California Institute of Technology, the University of California and the National Aeronautics and Space Administration. The Observatory was made possible by the generous financial support of the W.M. Keck Foundation. Data analysis were in part carried out on common use data analysis computer system at the Astronomy Data Center, ADC, of the National Astronomical Observatory of Japan.

REFERENCES

Baldwin J. A., Phillips M. M., Terlevich R., 1981, PASP, 93, 5
Bigiel F., Leroy A., Walter F., Brinks E., de Blok W. J. G., Madore B., Thornley M. D., 2008, AJ, 136, 2846
Brammer G. B., van Dokkum P. G., Coppi P., 2008, ApJ, 686, 1503
Brinchmann J., Pettini M., Charlot S., 2008, MNRAS, 385, 769
Brocklehurst M., 1971, MNRAS, 153, 471
Bruzual G., Charlot S., 2003, MNRAS, 344, 1000
Calzetti D., Armus L., Bohlin R. C., Kinney A. L., Koornneef J., Storchi-Bergmann T., 2000, ApJ, 533, 682
Chabrier G., 2003, PASP, 115, 763
Charlot S., Longhetti M., 2001, MNRAS, 323, 887
Coil A. L., et al., 2015, ApJ, 801, 35
Förster Schreiber N. M., et al., 2009, ApJ, 706, 1364
Gottlöber S., Klypin A., Kravtsov A. V., 2001, ApJ, 546, 223
Hayashi M., Kodama T., Tadaki K.-i., Koyama Y., Tanaka I., 2012, ApJ, 757, 15
Heiderman A., Evans II N. J., Allen L. E., Huard T., Heyer M., 2010, ApJ, 723, 1019
Holden B. P., et al., 2014, preprint, (arXiv:1401.5490)
Hollenbach D. J., Tielens A. G. G. M., 1999, Reviews of Modern Physics, 71, 173
Ichikawa T., et al., 2006, in Society of Photo-Optical Instrumentation Engineers (SPIE) Conference Series. , doi:10.1117/12.670078
Juneau S., Dickinson M., Alexander D. M., Salim S., 2011, ApJ, 736, 104
Juneau S., et al., 2014, ApJ, 788, 88
Kennicutt Jr. R. C., 1998, ARA&A, 36, 189
Kennicutt R. C., Evans N. J., 2012, ARA&A, 50, 531
Kodama T., Hayashi M., Koyama Y., Tadaki K.-i., Tanaka I., Shimakawa R., 2013, in Thomas D., Pasquali A., Ferreras I., eds, IAU Symposium Vol. 295, IAU Symposium. pp 74–77, doi:10.1017/S1743921313004353
Kriek M., van Dokkum P. G., Labbé I., Franx M., Illingworth G. D., Marchesini D., Quadri R. F., 2009, ApJ, 700, 221
Kriek M., et al., 2014, preprint, (arXiv:1412.1835)
Kriss G., 1994, Astronomical Data Analysis Software and Systems, 3, 437
Kruijssen J. M. D., Longmore S. N., 2014, MNRAS, 439, 3239
Kulas K. R., et al., 2013, ApJ, 774, 130
Lehnert M. D., Nesvadba N. P. H., Le Tiran L., Di Matteo P., van Driel W., Douglas L. S., Chemin L., Bournaud F., 2009, ApJ, 699, 1660

Liu X., Shapley A. E., Coil A. L., Brinchmann J., Ma C.-P., 2008, ApJ, 678, 758
Martin C. L., 1997, ApJ, 491, 561
Masters D., et al., 2014, ApJ, 785, 153
McLean I. S., et al., 2010, in Society of Photo-Optical Instrumentation Engineers (SPIE) Conference Series. p. 1, doi:10.1117/12.856715
McLean I. S., et al., 2012, in Society of Photo-Optical Instrumentation Engineers (SPIE) Conference Series. , doi:10.1117/12.924794
Nakajima K., Ouchi M., 2014, MNRAS, 442, 900
Oey M. S., Kennicutt Jr. R. C., 1997, MNRAS, 291, 827
Oey M. S., et al., 2007, ApJ, 661, 801
Osterbrock D. E., 1974, Astrophysics of gaseous nebulae
Peng C. Y., Ho L. C., Impey C. D., Rix H.-W., 2010, AJ, 139, 2097
Prescott M. K. M., et al., 2007, ApJ, 668, 182
Sanders R. L., et al., 2015, ApJ, 799, 138
Schmidt M., 1959, ApJ, 129, 243
Shapley A. E., et al., 2015, ApJ, 801, 88
Shimakawa R., Kodama T., Tadaki K.-i., Tanaka I., Hayashi M., Koyama Y., 2014, MNRAS, 441, L1
Shimakawa R., Kodama T., Tadaki K.-i., Hayashi M., Koyama Y., Tanaka I., 2015, MNRAS, 448, 666
Shirazi M., Brinchmann J., Rahmati A., 2014, ApJ, 787, 120
Steidel C. C., et al., 2014, ApJ, 795, 165
Storey P. J., Zeippen C. J., 2000, MNRAS, 312, 813
Suzuki R., et al., 2008, PASJ, 60, 1347
Tremonti C. A., et al., 2004, ApJ, 613, 898
Valentino F., et al., 2015, ApJ, 801, 132
Wuyts S., et al., 2011, ApJ, 742, 96

This paper has been typeset from a TEX/ LATEX file prepared by the author.